Polymer Chemistry

ROYAL SOCIETY OF CHEMISTRY

PAPER

Published on 01 July 2026

Cite this: *Polym. Chem.*, 2026, **17**, 3226

Effect of graphene oxide sheet size on pickering miniemulsion polymerization of styrene

Yue Zhang,[a] Yasemin Fadil,[a] Yuta Nishina,[b] Vipul Agarwal *[a,c] and Per B. Zetterlund *[a]

The effect of graphene oxide (GO) sheet size on the progression of Pickering miniemulsion polymerization of styrene was systematically investigated using two GO samples with lateral dimensions (~500 nm and 5–10 μm). Key parameters, including the presence of the conventional surfactant sodium dodecyl sulfate (SDS), GO loading, and initiator concentration, were investigated individually. Miniemulsion polymerization with GO was successfully conducted both in the absence and presence of SDS, with the addition of SDS leading to a significant rate enhancement attributed to SDS-induced secondary nucleation. In the presence of SDS, GO sheet size influenced polymerization behavior, and its effect on polymerization rate and monomer conversion exhibited opposite trends at different GO loadings. Small GO (~500 nm) led to higher conversion and faster rates at high GO loading (5 wt%), whereas large GO (5–10 μm) resulted in higher conversion and faster rates at low GO loading (0.5 wt%). This size-dependent effect became more pronounced at lower initiator concentration. Overall, while GO sheet size exhibited a measurable influence on polymerization behavior, the overall kinetics were primarily governed by SDS-induced secondary nucleation. These findings provide new insights into the role of GO lateral dimensions in miniemulsion polymerization and offer guidance for the design and synthesis of polymer/graphene (oxide) nanocomposites with tunable properties.

Received 29th April 2026,
Accepted 30th June 2026

DOI: 10.1039/d6py00414h

rsc.li/polymers

Introduction

Polymer/graphene oxide (GO) nanocomposites have attracted significant attention because of their multifunctional properties and straightforward fabrication.[1–4] Compared with graphene, GO is more favorable in the fabrication of nanocomposites due to its amphiphilic nature, structural tunability, and potential for mass production.[5–7] The presence of the hydrophilic oxygen-containing functional groups and the hydrophobic sp^2-hybridized basal plane enables good dispersibility of GO sheets in aqueous media and enhanced compatibility with polymers.[8,9] In addition, these surface functionalities have been reported to vary with lateral size.[10] Polymer/GO nanocomposites exhibit improved properties including thermal stability, electrical and thermal conductivity, mechanical strength, adsorption properties, barrier resistance, and electrochemical performance,[11–16] which can be further enhanced *via* thermal or chemical reduction of GO to conductive reduced GO (rGO).[17,18] Furthermore, the properties of polymer/GO nanocomposites can be readily tuned by adjusting the lateral size of the GO sheets.[19–22] For example, Wan *et al.* synthesized graphene aerogel–epoxy nanocomposites with tunable properties using GO sheets of different lateral sizes. They demonstrated that the GO size affects the morphology, structure, and pore sizes of the aerogel, thereby influencing the electromagnetic interference (EMI) shielding performance, electrical conductivity and mechanical properties.[19] Ramezanzadeh *et al.* showed that the size of *p*-phenylenediamine-functionalized GO affects its dispersion and interfacial interactions within epoxy matrices, consequently impacting the mechanical and anticorrosion performance of the resulting coatings.[20] In addition, GO size has been shown to influence the defect density and reduction efficiency to rGO,[23] as well as the orientation and alignment of GO sheets in poly (vinylidene fluoride-*co*-hexafluoropropylene) nanocomposites, thereby affecting the thermal and electrical conductivity.[21] These tunable and versatile properties make polymer/GO nanocomposites promising for applications in energy storage and sensing, EMI shielding, corrosion protection and biomedical settings.[24–28]

Among the various fabrication methods, aqueous emulsion-based polymerization techniques are particularly attrac-

[a]*Cluster for Advanced Macromolecular Design, School of Chemical Engineering, The University of New South Wales, Sydney, NSW, 2052, Australia.*
E-mail: agarwalvipul84@gmail.com, p.zetterlund@unsw.edu.au
[b]*Research Core for Interdisciplinary Sciences, Okayama University, Okayama, 700-8530, Japan*
[c]*Department of Materials Science and Engineering, Monash University, Clayton, VIC, 3800, Australia*

tive for the preparation of polymer/GO nanocomposites.[29] These approaches, for example, miniemulsion polymerization and physical mixing, offer advantages including environmental friendliness, scalability, and applicability to a broad range of monomers.[30] Importantly, it has been demonstrated by us that the arrangement and distribution of GO sheets within the polymer matrix significantly influence the electrical conductivity of the resulting polymer/GO nanocomposites, which can be readily tuned by adjusting the nanocomposite synthesis strategy,[31] or in the case of miniemulsion polymerization, by adjusting the surfactant amount.[32] Physical mixing involves blending aqueous dispersions of polymer nanoparticles and GO, respectively, where film formation can induce self-alignment of GO sheets into thick well-defined domains that facilitate electron transport.[31,33] In contrast, in miniemulsion polymerization, the amphiphilic nature of GO allows it to act as a surfactant, stabilizing the oil–water interface and promoting the formation of polymer nanoparticles armored with GO sheets.[34–36] However, adsorption of GO at the particle interface may restrict the self-assembly of GO sheets during film formation, resulting in a network composed of many small channels with numerous "dead ends" within the polymer matrix, thereby limiting electron transport.[31] Increasing the sodium dodecyl sulfate (SDS) concentration to 7 wt% can mitigate this effect, leading to the formation of interconnected and linear domains of self-assembled GO sheets.[32] Consequently, miniemulsion polymerization enables partially controlled positioning of GO at the particle interfaces, providing a platform for nanoengineering the composite structure.

GO typically exists with a broad and ill-defined size distribution, and the influence of GO size on miniemulsion polymerization remains largely unexplored. The variations in lateral GO size may influence key aspects of miniemulsion polymerization systems, including droplet stabilization, particle nucleation, and growth mechanisms. Therefore, understanding the role of GO size in miniemulsion polymerization is crucial, particularly with respect to particle formation pathways and polymerization kinetics. In this work, well-defined GO sheets of distinct lateral dimensions are employed to systematically investigate the effect of GO size on the progression of Pickering miniemulsion polymerization of styrene. Accordingly, this study investigates Pickering miniemulsion polymerization of styrene in the presence of graphene oxide (St/GO) using two GO samples with markedly different lateral dimensions, namely small GO (~500 nm) and large GO (5–10 μm). To assist in understanding the underlying mechanisms, additional parameters including GO loading, the presence or absence of surfactant (SDS), and initiator concentration were varied. The effects of these variables on the visual appearance of the St/GO miniemulsions and latexes, droplet and particle size, monomer conversion, and molecular weight were examined. By clarifying how GO lateral size influences polymer particle formation and polymerization behavior, this study provides new insight into GO-based Pickering miniemulsion polymerization and offers useful guidance for the design of polymer/GO nanocomposites with tailored structures and properties.

Materials and methods

Materials

Styrene (St, Sigma-Aldrich, 99%) was purified by passing through a column of activated basic aluminum oxide (Sigma-Aldrich) to remove the inhibitor. Azobisisobutyronitrile (AIBN, Sigma-Aldrich, 0.2 M in toluene) was recrystallized in water prior to use. Hexadecane (HD, Sigma-Aldrich, 99%) and sodium dodecyl sulfate (SDS, Sigma-Aldrich, 99%) were used as received. The water used in all experiments was Milli-Q water. Natural graphite (SP 1 grade, Bay Carbon Inc.), concentrated sulfuric acid (95%, Wako Pure Chemical Industries, Ltd), and potassium permanganate ($KMnO_4$, Wako Pure Chemical Industries, Ltd) were used for GO preparation.

Graphene oxide

GO dispersions of two different sizes (approximately 500 nm and 5–10 μm, referred to as small GO and large GO, respectively) were prepared by a combination of a modified Hummers' method and liquid-phase jet milling. Briefly, 10 g of natural graphite was dispersed in 30 mL of concentrated sulfuric acid and cooled in an ice-water bath. Then, 30 g of $KMnO_4$ was added dropwise while maintaining the reaction temperature below 50 °C, and the mixture was stirred at 35 °C for 2 h. The reaction mixture was then diluted with cold water (~50 mL), followed by the addition of aqueous H_2O_2 until gas evolution was no longer observed (~5 mL). The resulting product was purified by repeated centrifugation until the pH of the supernatant exceeded 3. Finally, the concentration was adjusted to 1 wt%, and the dispersion was subjected to mild mechanical stirring (for large GO) or wet-type jet milling (for small GO).

Pickering miniemulsion polymerization of St with GO

Miniemulsion polymerizations were carried out according to the recipes in Table 1, using two sizes of GO, respectively

Table 1 Recipes for miniemulsion polymerization of St at 70 °C for 24 h using two different sizes of GO (small GO and large GO, respectively)

	GO		AIBN		SDS	
Experiment	wt% [a]	g	mol L^{-1} [b]	g	wt% [c]	g
A0	0	0	0.25	0.05	1	0.01
A1	5	0.05	0.25	0.05	1	0.01
A2	5	0.05	0.25	0.05	0	0
B1	5	0.05	0.025	0.005	1	0.01
B2	5	0.05	0.025	0.005	0	0
A3	0.5	0.005	0.25	0.05	1	0.01
B3	0.5	0.005	0.025	0.005	1	0.01

[a] wt% relative to monomer. [b] mol L^{-1} relative to organic phase. [c] wt% relative to organic phase.

(small GO and large GO). An aqueous GO dispersion (15 g of water) was ultrasonicated on ice for 10 min using a Branson Digital Sonifier at 70% amplitude. The organic phase was prepared by mixing St (1.05 g), AIBN, HD (0.0525 g) and SDS. The pre-sonicated aqueous GO dispersion was then added to the organic phase. The resulting mixture was magnetically stirred on ice for 15 min, followed by ultrasonication on ice for another 10 min (70% amplitude) to form a miniemulsion. The miniemulsion was subsequently degassed by nitrogen for 20 min. Polymerization was subsequently conducted in a sealed 25 mL glass vial at 70 °C for 24 h under constant magnetic stirring. Samples were collected at specific time points: 30 min, 1, 2, 3, 4, 6, and 24 h. The precise amounts of GO, AIBN and SDS used in each experiment are detailed in Table 1. The SDS concentration used was below the critical micelle concentration (CMC; 8 mM).[37]

Dynamic light scattering (DLS)

Z-Average diameters (Z_{av}) of miniemulsion droplets (prior to polymerization) and polymer particles were determined by DLS using Malvern Zetasizer Nano Series equipped with DTS software. Measurements were performed with a 4 mW He–Ne laser (λ = 633 nm) at 25 °C and a scattering angle of 173°. Each sample was prepared by diluting a drop of miniemulsion or latex (approximately 10^{-4} mg mL^{-1}) with Milli-Q water (~5 mL). Three measurements were conducted on each sample.

Gravimetric analysis

Monomer conversions were determined by gravimetric analysis. Approximately 1.5 g of polymer latex was placed in a pre-weighed aluminum pan and dried in a vacuum oven at 30 °C for 24 h. The mass of the dried polymer was then used to calculate the monomer conversion.

Transmission electron microscopy (TEM)

TEM images of GO were acquired using a JEOL F200 TEM operating at an accelerating voltage of 200 kV. Images were recorded *via* Gatan CCD imaging software. TEM samples were prepared by dropping 10 μL of diluted GO dispersions onto carbon- and formvar-supported copper grids.

Gel permeation chromatography (GPC)

Number-average molecular weights (M_n), weight-average molecular weight (M_w) and molecular weight distributions (MWDs) were determined using GPC. The GPC system was equipped with an SIL-10AD autoinjector, an LC10AT pump, a DGU-12A degasser, a CTO-10A column oven, and an RID10A differential refractive index detector. *N*,*N*-Dimethylacetamide (DMAc) was used as the mobile phase at 50 °C, with a constant flow rate of 1 mL min^{-1}. The system was calibrated using linear polystyrene standards ranging from 500 to 10^6 g mol^{-1}. Approximately 2 mg of dried polymer nanocomposite latex was dissolved in 1 ml of DMAc, followed by filtering through a 0.45 μm syringe filter to remove impurities and GO prior to injection.

X-ray photoelectron spectroscopy (XPS)

The chemical composition of GO samples with different sizes was analyzed by XPS using a Thermo Scientific ESCALAB250Xi spectrometer. The instrument was equipped with a monochromatic Al Kα X-ray source (1486.68 eV) operated at 120 W (13.8 kV × 8.7 mA).

Results and discussion

Compositional analysis of GO with different sheet size

The overall objective of the present work has been to explore how the progression of Pickering miniemulsion polymerization of St using GO is influenced by GO sheet size. To this end, "small" and "large" GO were prepared as described in the Experimental section – these are hereafter referred to as SGO and LGO, respectively. Transmission electron microscopy (TEM) and scanning electron microscope (SEM) were performed to determine the lateral size of the SGO and LGO sheets.

The SGO sheets exhibited lateral dimensions of approximately 500 nm, whereas the LGO sheets ranged from 5–10 μm (Fig. 1 and 2). X-ray photoelectron spectroscopy (XPS) was conducted to gain information on elemental compositions and specific functional groups of SGO and LGO (Fig. S1, Table S1 and Table 2). The XPS peak fitting results were organized into Table S1 and Table 2. The elemental composition is summarized in Table S1 (used to calculate the atomic C/O ratios), while Table 2 presents the atomic percentages of carbon chemical states in the samples. The atomic C/O ratio was 2.37 for SGO and 3.37 for LGO. The C/O ratio of SGO is consistent with typical values reported for GO, including GO prepared and used in our previous studies (1.83–2.01)[18,34,36,38] and in other studies (1.34–2.77).[23,39–41] The C/O ratio of LGO exceeds this range, indicating a lower oxidation level. Under the same oxidation conditions, larger GO sheets generally exhibit a higher C/O ratio due to the lower proportion of edge-located oxygen-containing groups (due to less edge per sheet the larger the sheet). The atomic percentage of ketone groups (C═O) increased with GO size, from 13.9% for SGO to 17.8% for LGO, while the content of hydroxyl and epoxide groups (C–OH and C–O–C) decreased from 7.3% to 3.6%. Although ketone groups were the most dominant functional groups in both SGO and LGO, a notable presence of carboxylic groups (COOH) was also observed at 1.5% for SGO to 2.6% for LGO. These trends highlight the differences in oxidation state and surface functionality between SGO and LGO.

St/GO miniemulsion polymerization at high initiator concentration

Miniemulsion polymerizations of St were first conducted using SGO and LGO, respectively, at 5 wt% relative to St. The polymerizations were initiated with 0.25 M AIBN (concentration relative to the organic phase), conducted both in the absence and presence of SDS (1 wt% relative to the organic phase), following the recipes listed in Table 1 (Experiments A1 and A2). The pH of the miniemulsion before polymerization was 2.3 with and without SDS, *i.e.* the presence of SDS does not signifi-

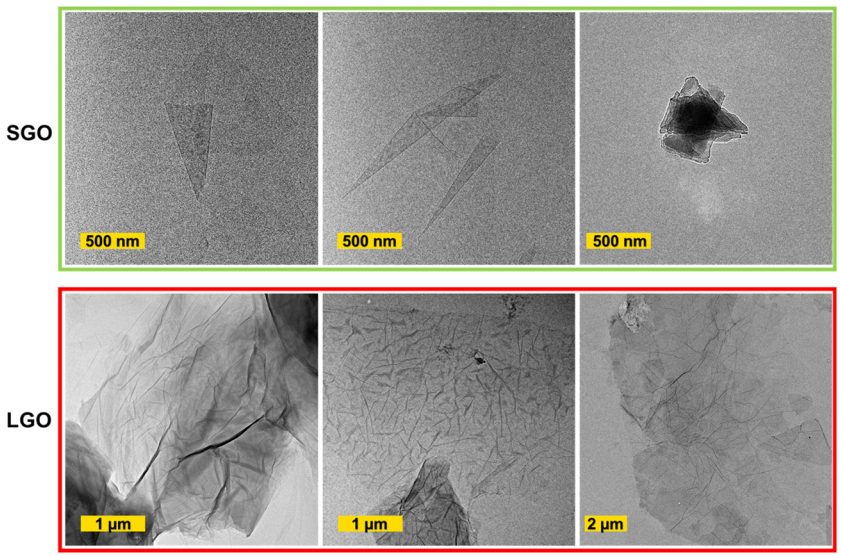

Fig. 1 TEM images of SGO (scale bar is 500 nm) and LGO (scale bar is 1 μm and 2 μm).

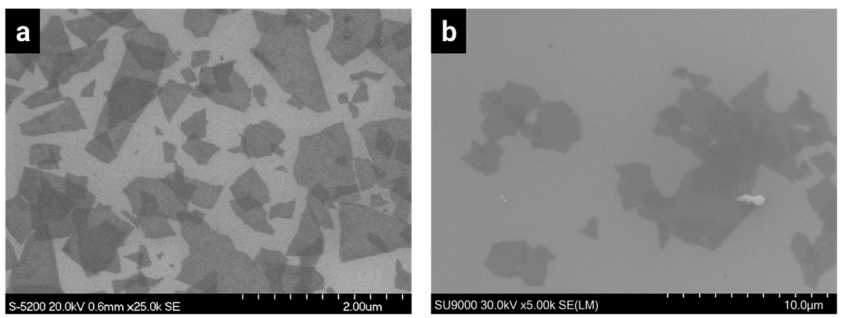

Fig. 2 SEM images of (a) SGO and (b) LGO (scale bars: 2 and 10 μm, respectively).

Table 2 Atomic percentages of carbon chemical states in SGO and LGO derived from XPS analysis

Samples	Atomic C/O ratio	Peak groups	Binding energy (eV)	Atomic conc.[a] (%)
SGO	2.37	C–C/C=C	284.8	40.4
		C–OH/C–O–C	285.6	7.3
		C=O	287.4	13.9
		COOH	289.0	1.5
LGO	3.37	C–C/C=C	284.8	51.3
		C–OH/C–O–C	285.9	3.6
		C=O	287.1	17.8
		COOH	288.9	2.6

[a] Atomic percentages of carbon functional groups are reported relative to the total number of all detected atoms (C, O, N, S, Si, *etc.*), which sum to 100%.

cantly affect the pH. Notably, this AIBN concentration is far higher than what would be considered normal for polymerization of St – it has previously been reported by us that Pickering miniemulsion polymerization of St (and copolymerization involving St) using GO leads to significant retardation for reasons that remain to be clarified.[34] When using other vinyl monomers in Pickering miniemulsion polymerization, such retardation has not been observed.[35] To date, we have observed this retardation using both very small GO prepared from graphite nanofibers (size of approx. 100 nm)[34,35,42] as well as commercially available GO of average size 300 nm.[36,43]

The size of GO had no significant effect on the visual appearance of the St/GO miniemulsions before polymerization, but clear differences emerged after polymerization onset in the presence of SDS. Latexes with SGO turned grey/blue within 0.5 h of polymerization and maintained this color throughout the polymerization. In contrast, latexes prepared with LGO also appeared grey/blue after polymerization had begun, but gradually faded to brown by the end of the polymerization (Fig. 3, A1). In the absence of SDS, no noticeable difference between SGO and LGO was observed; all latexes exhibited an initial brown color that darkened over time (Fig. 3, A2). Further work is required to unearth the origin(s) of these marked differences in appearance.

For both SGO and LGO, the addition of SDS significantly reduced droplet/particle sizes (Fig. S4, A1 and A2). Interestingly,

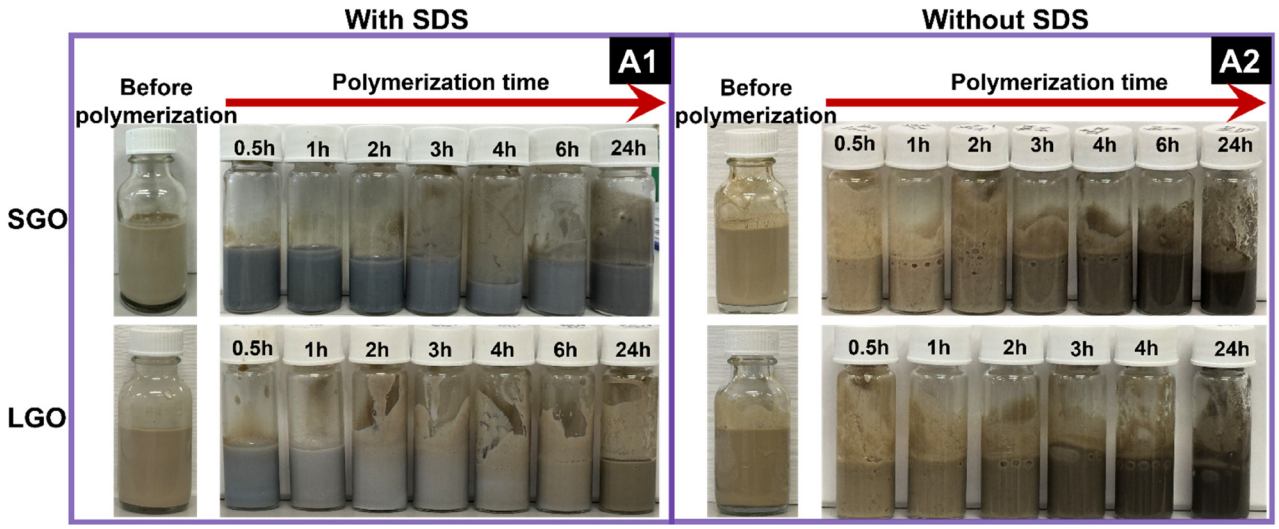

Fig. 3 Photographs of 0.25 M AIBN-initiated miniemulsion polymerization of St at 70 °C for 24 h with 5 wt% GO relative to St, in the presence (A1) and absence of SDS (A2) at different polymerization times; before polymerization, 0.5 h, 1 h, 2 h, 3 h, 4 h, 6 h, and 24 h (both SGO and LGO were used in the recipes A1–A2 in Table 1).

in the presence of SDS, SGO resulted in particles smaller than the initial droplet sizes, whereas LGO led to the formation of larger particles relative to the original droplets (Table 3). It should be noted that interpreting DLS data in this system is challenging, as DLS theory applies exclusively to spherical objects. GO sheets are dispersed in the aqueous phase and interact with polymer particles, thereby affecting the light scattering. The particle size trends observed with and without SDS for both SGO and LGO are consistent with our previous work (using GO of approximately 300 nm) and are attributed to secondary nucleation in the presence of SDS. In the absence of SDS, large polymer particles "armoured" with GO sheets are formed from large droplets stabilized by GO. SDS facilitates secondary nucleation including nucleation *via* GO sheets stabilized by SDS, and homogeneous nucleation stabilized solely by SDS. This highlights the important role of SDS in enabling secondary nucleation, which in turn influences both droplet and particle sizes.[36]

Table 3 *Z*-Average diameters (Z_{av}) of droplets/particles for 0.25 M and 0.025 M AIBN initiated miniemulsion polymerizations of St with 0.5 wt% GO in the presence of SDS, or 5 wt% GO with and without SDS (both SGO and LGO were used in all polymerizations)

GO[a]	SDS[b]	AIBN[c]	GO size	Conversion[d] (%)	Droplet Z_{av}[f] (nm)	Particle Z_{av}[g] (nm)
5	1	0.25	SGO	93	283	105
			LGO	83	431	455
		0.025	SGO	91	245	172
			LGO	88	266	279
	0	0.25	SGO	34	596	—
			LGO	49[e]	631	—
		0.025	SGO	14	712	—
			LGO	28	519	—
0.5	1	0.25	SGO	91	453	82
			LGO	93	331	83
		0.025	SGO	85	563	91
			LGO	96	199	92
0	1	0.25	—	88	250	77

[a] wt % relative to monomer. [b] wt% relative to organic phase. [c] mol L^{-1} relative to organic phase. [d] Monomer conversion at 6 h polymerization. [e] Monomer conversion at 4 h polymerization. [f] Droplet size of miniemulsions before polymerization. [g] Particle size of latexes after 6 h polymerization.

There was a significant enhancement in polymerization rate in the presence of SDS for both SGO and LGO (Fig. 4A). Although the SGO and LGO systems exhibited similar polymerization rates, higher conversions were achieved at longer times for SGO in the presence of SDS, whereas LGO led to higher conversion in the absence of SDS. However, these differences between GO sizes were minor compared to the pronounced effect of SDS. In addition, the presence of SDS also caused a noticeable shift toward higher MWs, while GO size showed no significant effect on the MWs (Fig. 5A). These effects on polymerization rates and MWDs are consistent with what we have previously reported. SDS-induced secondary nucleation promotes a partial transition to emulsion polymerization characteristics, where radical segregation within small particles reduces termination rates, thereby increasing both polymerization rate and MW.[36] It is apparent that these fundamental kinetic effects imparted by the presence of SDS are only marginally affected by GO size, despite the very significant difference in size between SGO and LGO.

St/GO miniemulsion polymerization at low initiator concentration

The polymerizations described above employed a very high AIBN concentration (0.25 M) to overcome the known retardation effect of GO.[34,35] Additional miniemulsion polymerizations were conducted using a more normal AIBN concentration (0.025 M), according to the recipes in Table 1 (B1 and B2).

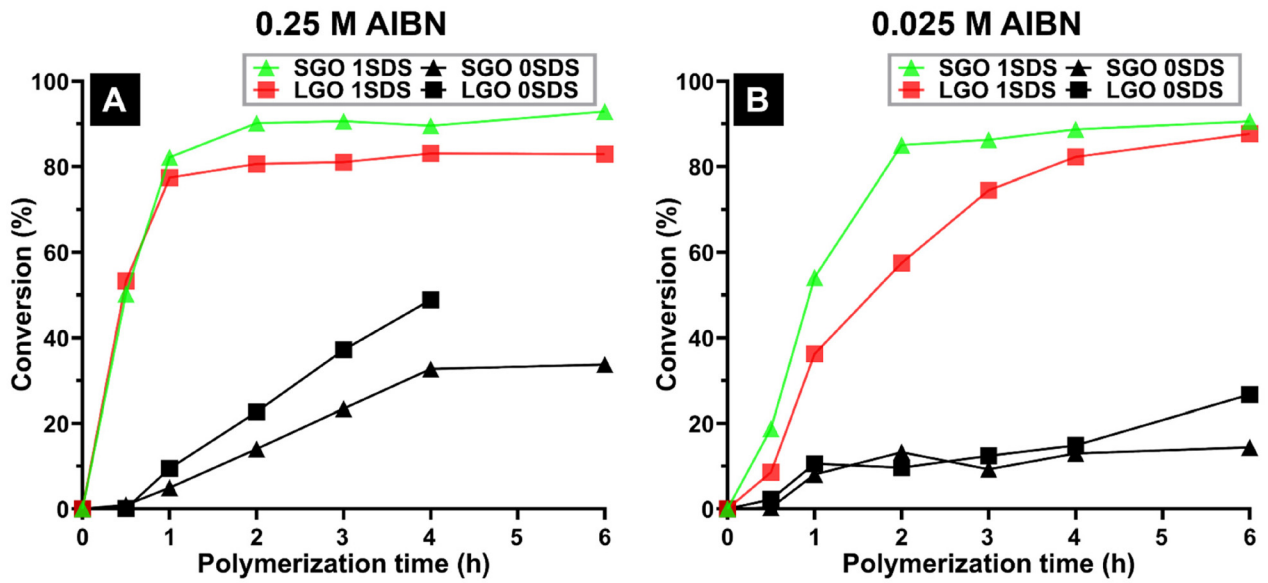

Fig. 4 Monomer conversion *vs.* time data for (A) 0.25 M and (B) 0.025 M AIBN-initiated miniemulsion polymerizations of St at 70 °C with 5 wt% SGO (triangle) and LGO (square) relative to St, in the presence (green and red lines) and absence of SDS (black line) (Recipes A1–A2 and B1–B2 in Table 1 correspond to A and B, respectively).

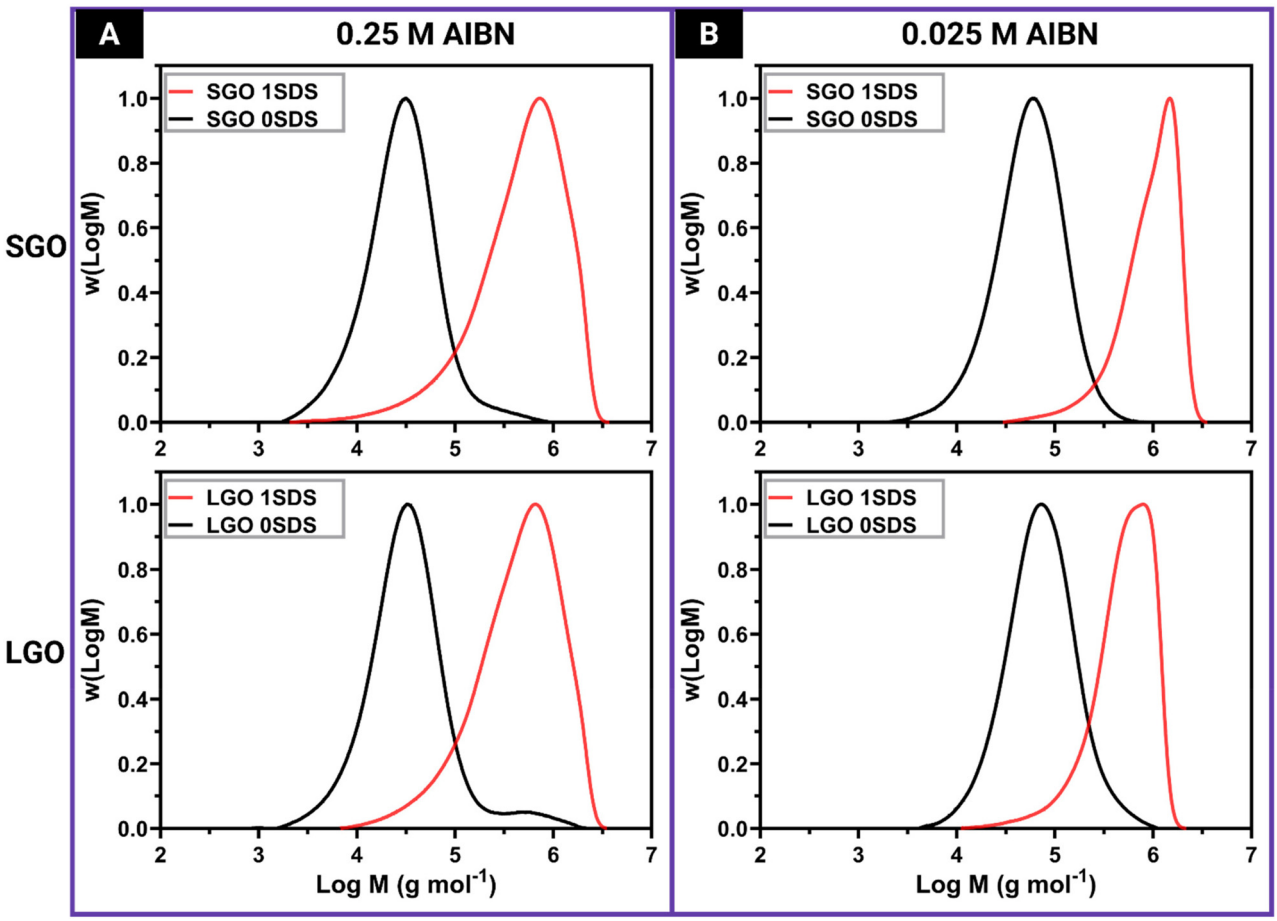

Fig. 5 MWDs for miniemulsion polymerizations of St at 70 °C using (A) 0.25 M and (B) 0.025 M AIBN, with 5 wt% GO relative to St, in the presence (red curve) and absence of SDS (black curve) (Recipes A1–A2 and B1–B2 in Table 1 correspond to A and B, respectively).

Regarding the effect of GO size on the evolution of the appearance of the latexes over time, a similar trend was observed as for the high initiator concentration. However, the blue color intensity of the latexes prepared with SDS was lower for both SGO and LGO. In both cases, the blue color gradually faded with increasing polymerization time and eventually disappeared, resulting in brown-colored latexes after 24 h of polymerization (Fig. S2, B1). For the latexes prepared without SDS, the evolution of the appearance followed a similar pattern to that observed at 0.25 M AIBN (Fig. S2, B2).

At this lower initiator concentration, the trends in droplet/particle sizes, polymerization rates, monomer conversions, and MWs with and without SDS (Fig. 4, 5 and Table 3) were consistent with those observed at higher initiator concentration. The presence of SDS led to higher rates and MWs and lower droplet/particle sizes, consistent with SDS-induced secondary nucleation also at lower initiator concentration. Notably, reducing the initiator concentration magnified the influence of GO size in the presence of SDS; SGO led to higher polymerization rate than LGO, although comparable conversions were ultimately achieved. In contrast, in the absence of SDS, size-dependent differences were effectively eliminated, with both SGO and LGO resulting in comparable rates and conversions. This indicated that lowering the initiator concentration amplified the effect of GO size only when SDS was present, while in SDS-free systems, GO size had relatively minor influence on polymerization rates (Fig. 4B).

The effect of initiator concentration on MW was similar for SGO and LGO, with the MWDs generally shifting to higher MWs at the lower initiator concentration, consistent with expectation for a radical polymerization (Fig. S6).

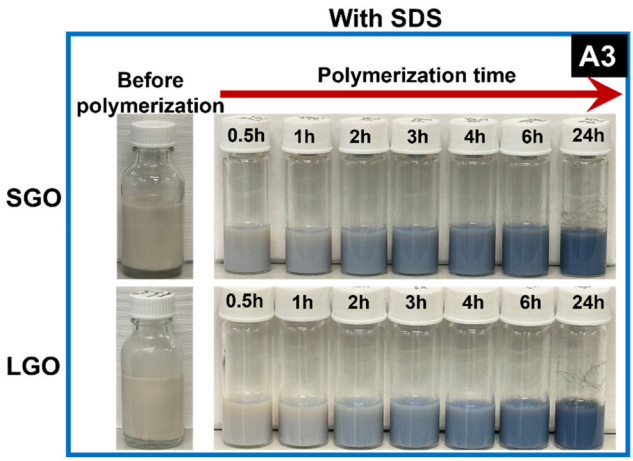

Fig. 6 Photographs of 0.25 M AIBN-initiated miniemulsion polymerization of St at 70 °C for 24 h with 0.5 wt% GO relative to St in the presence of SDS at different polymerization times: before polymerization, 30 min, 1 h, 2 h, 3 h, 4 h, 6 h, and 24 h (both SGO and LGO were used in recipes A3 in Table 1).

St/GO miniemulsion polymerization at reduced GO loading

To further investigate the effect of GO size on the polymerization in the presence of SDS, additional miniemulsion polymerizations were conducted with a lower GO loading (0.5 wt% relative to St). Both SGO and LGO were used at two initiator concentrations (0.25 M and 0.025 M AIBN), following the recipes in Table 1 (A3 and B3).

Lowering the GO loading produced less brown (more whitish) St/GO miniemulsions that gradually turned blue after polymerization onset, with no significant difference between SGO and LGO. However, the initiator concentration had a more pronounced effect, with a less intense blue color at the lower initiator concentration (Fig. 6 and Fig. S3). At 0.5 wt%

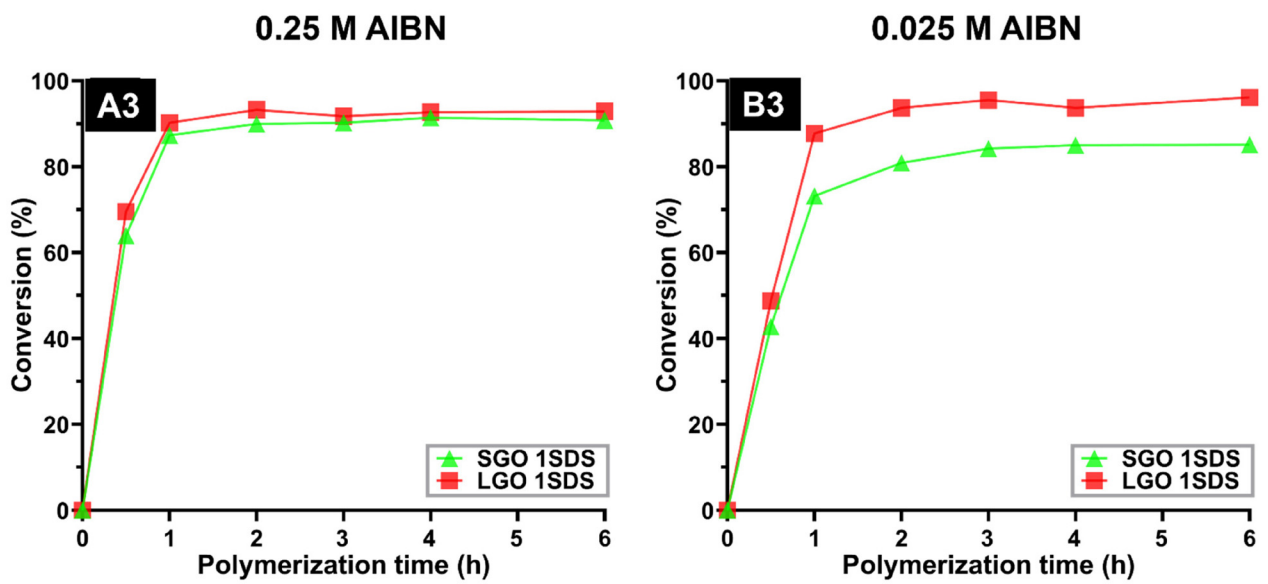

Fig. 7 Monomer conversion *vs.* time data for (A3) 0.25 M and (B3) 0.025 M AIBN-initiated miniemulsion polymerizations of St at 70 °C with 0.5 wt% SGO (triangle) and LGO (square) relative to St, in the presence of SDS (recipes A3 and B3 in Table 1).

GO, much smaller particles were formed (<100 nm) than at high GO loading for both SGO and LGO, which can be attributed to SDS induced secondary nucleation, primarily *via* homogeneous nucleation.[36] At this lower GO loading, SGO and LGO also led to comparable polymerization rates, but a reversed size-dependent conversion trend was observed, with LGO reaching higher conversions at longer times, particularly at the lower initiator concentration (Fig. 7).

The lower GO loading resulted in an increase in polymerization rates for both GO sizes (Fig. 8), with the largest enhancement observed for LGO at 0.025 M AIBN (Fig. 8, B-L), highlighting the stronger influence of GO concentration under lower initiator and LGO condition. Similar to the 5 wt% GO systems, GO size had no effect on MWDs, and reducing the GO loading minimally impacted the MWDs (Fig. S6).

The effect of initiator concentration on both polymerization rates and MWs was consistent across the two GO loadings, with lower initiator concentration resulting in slower polymerization but higher MWs, consistent with the fundamental characteristics of radical polymerizations.

SDS-induced secondary nucleation mechanism

As reported in our previous work,[36] the addition of SDS introduces additional nucleation pathways, including nucleation of droplets stabilized jointly by GO and SDS (type ii), nucleation involving GO sheets stabilized by SDS (type iii), and homogeneous nucleation where oligomeric radicals precipitate in the aqueous phase and are stabilized by SDS (type iv). Among these, the latter two pathways can be considered secondary nucleation, imparting characteristics of emulsion polymerization such as accelerated polymerization, higher monomer conversions and increased molecular weights due to radical compartmentalization within small polymer particles (segregation effect).[44,45] In St/GO/SDS Pickering miniemulsion

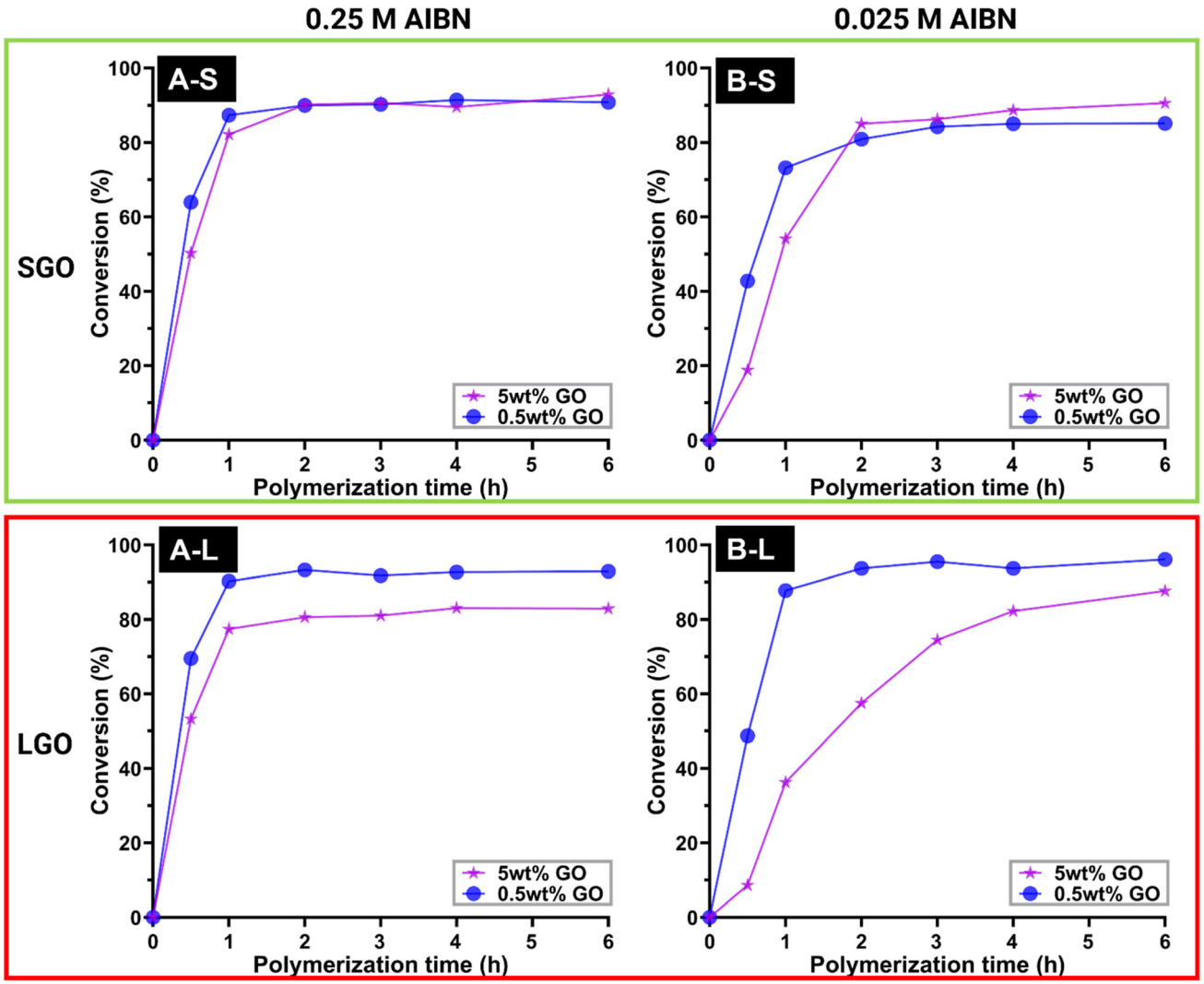

Fig. 8 Monomer conversion *vs.* time for 0.25 M (A-S, A-L) and 0.025 M (B-S, B-L) AIBN-initiated miniemulsion polymerizations of St at 70 °C, with 5 wt% (purple star) and 0.5 wt% (blue circle) relative to St in the presence of SDS (both SGO (green frame) and LGO (red frame) were used in all miniemulsion polymerizations).

systems, smaller particles are mainly formed *via* type iv nucleation, whereas larger particles arise from type iii nucleation. At lower GO loadings, type iv nucleation dominates, leading to the formation of small particles, while at higher GO loadings, type ii and iii nucleation become more favored due to the greater number of free GO sheets in the aqueous phase. Initiator concentration also plays a role. At low initiator concentrations, type iv nucleation is more evident whereas at high concentration types i and ii nucleation dominate due to rapid initiation within large monomer droplets.

The effects of GO size on the kinetics of Pickering miniemulsion polymerization of St in the present work can largely be explained by invoking the secondary nucleation mechanism described above. In the presence of SDS at 5 wt% GO, DLS analysis showed that SGO produced particles smaller than the initial droplets, whereas LGO produced particles of comparable size to the original droplets. Despite similar polymerization rates, SGO achieved higher conversions than LGO at longer times, with the difference becoming more pronounced at lower initiator concentration. It can be speculated that these results may be explained by the stronger contribution of homogeneous nucleation (type iv) in the case of SGO, especially at low initiator concentration, while LGO primarily undergoes type ii and iii nucleation.

At 0.5 wt% GO, both SGO and LGO produced particles smaller than the initial droplets, reflecting an increased role of homogeneous nucleation (type iv) relative to 5 wt% GO loading. Although reversed size-dependent conversion trends were observed at lower GO loading, the overall difference between SGO and LGO was less pronounced, as type iv nucleation dominates at such low GO loading and produces small particles regardless of GO size, thereby diminishing GO size-dependent effects.

The SGO systems showed similar polymerization rates and conversions across different GO loadings, while LGO showed higher rates and higher conversions at lower GO loading (Fig. 8). In both cases, the effect of GO loading became more pronounced at lower initiator concentration. It is proposed that these observations can be explained by that for SGO, the relative contribution of nucleation pathways remains similar between high and low GO loadings. However, LGO shows a stronger dependence on system conditions, with type ii and iii nucleation dominating at high GO loading and initiator concentration but shifting toward type iv nucleation as both parameters are reduced.

Conclusions

In this work, two different sizes of GO sheets including SGO (~500 nm) and LGO (5–10 μm) were used to investigate the effect of GO size on the kinetics of Pickering miniemulsion polymerization of St under varying conditions (SDS addition, initiator concentration, and GO loading).

When GO nanosheets were used as the sole surfactant, pronounced retardation effects were observed for both sizes, which was largely alleviated upon SDS addition due to SDS-induced secondary nucleation.

In the presence of SDS (at amounts well below the CMC), SGO and LGO resulted in comparable polymerization rates, with size-dependent differences emerging at longer polymerization times – SGO led to higher conversions at higher GO loading, while LGO gave higher conversions at lower GO loading. GO loadings also influenced polymerization efficiency, with lower GO loading leading to an enhancement in polymerization rates and monomer conversions, particularly for LGO at lower initiator concentration. In contrast to the effect of SDS, which significantly increased MWs, different GO sizes and loadings had negligible impact on MWs. Therefore, despite the substantial size difference between SGO and LGO, the fundamental kinetics driven by SDS-induced secondary nucleation showed only minor dependence on GO size.

In conclusion, this work illustrates how GO size affects the kinetics of Pickering miniemulsion polymerization and provides useful insights for the design and synthesis of polymer/graphene (oxide) nanocomposites.

Conflicts of interest

The authors declare no conflicts of interest.

Data availability

The data that supports the findings of this study are available in the supplementary information (SI) of this article.

Acknowledgements

The authors acknowledge the scientific and technical assistance of the Surface Analysis Laboratory (SAL) and the Electron Microscope Unit (EMU) within the Mark Wainwright Analytical Centre (MWAC) at UNSW Sydney.

References

1 A. T. Smith, A. M. LaChance, S. Zeng, B. Liu and L. Sun, Synthesis, properties, and applications of graphene oxide/reduced graphene oxide and their nanocomposites, *Nano Mater. Sci.*, 2019, **1**(1), 31–47.
2 R. Shah, A. Kausar, B. Muhammad and S. Shah, Progression from graphene and graphene oxide to high performance polymer-based nanocomposite: a review, *Polym.-Plast. Technol. Eng.*, 2015, **54**(2), 173–183.
3 Z. U. Khan, A. Kausar, H. Ullah, A. Badshah and W. U. Khan, A review of graphene oxide, graphene buckypaper, and polymer/graphene composites: Properties and fabrication techniques, *J. Plast. Film Sheeting*, 2016, **32**(4), 336–379.
4 Z. Shahryari, M. Yeganeh, K. Gheisari and B. Ramezanzadeh, A brief review of the graphene oxide-

based polymer nanocomposite coatings: preparation, characterization, and properties, *J. Coat. Technol. Res.*, 2021, **18**(4), 945–969.
5 H. Li, S. Xue, Y. Shang, J. Li and X. Zeng, Research and application progress based on the interfacial properties of graphene oxide, *Adv. Mater. Interfaces*, 2020, **7**(21), 2000881.
6 Y. Nishina and S. Eigler, Chemical and electrochemical synthesis of graphene oxide – a generalized view, *Nanoscale*, 2020, **12**(24), 12731–12740.
7 Y. Nishina, Mass production of graphene oxide beyond the laboratory: bridging the gap between academic research and industry, *ACS Nano*, 2024, **18**(49), 33264–33275.
8 L. J. Cote, J. Kim, V. C. Tung, J. Luo, F. Kim and J. Huang, Graphene oxide as surfactant sheets, *Pure Appl. Chem.*, 2010, **83**(1), 95–110.
9 J. Kim, L. J. Cote, F. Kim, W. Yuan, K. R. Shull and J. Huang, Graphene Oxide Sheets at Interfaces, *J. Am. Chem. Soc.*, 2010, **132**(23), 8180–8186.
10 Y. Y. Khine, X. Ren, D. Chu, Y. Nishina, T. Foller and R. Joshi, Surface functionalities of graphene oxide with varying flake size, *Ind. Eng. Chem. Res.*, 2022, **61**(19), 6531–6536.
11 T. H. Min and H. J. Choi, Synthesis of poly (methyl methacrylate)/graphene oxide nanocomposite particles via Pickering emulsion polymerization and their viscous response under an electric field, *Macromol. Res.*, 2017, **25**, 565–571.
12 B. Ramezanzadeh, E. Ghasemi, M. Mahdavian, E. Changizi and M. M. Moghadam, Covalently-grafted graphene oxide nanosheets to improve barrier and corrosion protection properties of polyurethane coatings, *Carbon*, 2015, **93**, 555–573.
13 W. Du, Z. Zhang, H. Su, H. Lin and Z. Li, Urethane-functionalized graphene oxide for improving compatibility and thermal conductivity of waterborne polyurethane composites, *Ind. Eng. Chem. Res.*, 2018, **57**(21), 7146–7155.
14 M. Abutalib, Insights into the structural, optical, thermal, dielectric, and electrical properties of PMMA/PANI loaded with graphene oxide nanoparticles, *Phys. B*, 2019, **552**, 19–29.
15 R. Khan and Y. Nishina, Grafting conductive polymers on graphene oxide through cross-linker: a stepwise approach, *J. Mater. Chem. A*, 2020, **8**(27), 13718–13724.
16 R. Kimura, P. Ferré-Pujol and Y. Nishina, Grafting-through functionalization of graphene oxide with cationic polymers for enhanced adsorption of anionic dyes and viruses, *Carbon*, 2025, **238**, 120296.
17 V. Agarwal and P. B. Zetterlund, Strategies for reduction of graphene oxide–A comprehensive review, *Chem. Eng. J.*, 2021, **405**, 127018.
18 N. Maslekar, Y. Fadil, P. B. Zetterlund and V. Agarwal, Maintaining Colloidal Stability of Polymer/Reduced Graphene Oxide Nanocomposite Aqueous Dispersions Produced via In Situ Reduction of Graphene Oxide for the Preparation of Electrically Conductive Coatings, *ACS Appl. Nano Mater.*, 2023, **6**(7), 5177–5186.
19 Y.-J. Wan, S.-H. Yu, W.-H. Yang, P.-L. Zhu, R. Sun, C.-P. Wong and W.-H. Liao, Tuneable cellular-structured 3D graphene aerogel and its effect on electromagnetic interference shielding performance and mechanical properties of epoxy composites, *RSC Adv.*, 2016, **6**(61), 56589–56598.
20 B. Ramezanzadeh, G. Bahlakeh, M. M. Moghadam and R. Miraftab, Impact of size-controlled p-phenylenediamine (PPDA)-functionalized graphene oxide nanosheets on the GO-PPDA/Epoxy anti-corrosion, interfacial interactions and mechanical properties enhancement: Experimental and quantum mechanics investigations, *Chem. Eng. J.*, 2018, **335**, 737–755.
21 P. Kumar, S. Yu, F. Shahzad, S. M. Hong, Y.-H. Kim and C. M. Koo, Ultrahigh electrically and thermally conductive self-aligned graphene/polymer composites using large-area reduced graphene oxides, *Carbon*, 2016, **101**, 120–128.
22 J. Kim, S. W. Kim, H. Yun and B. J. Kim, Impact of size control of graphene oxide nanosheets for enhancing electrical and mechanical properties of carbon nanotube–polymer composites, *RSC Adv.*, 2017, **7**(48), 30221–30228.
23 P. Kumar, F. Shahzad, S. Yu, S. M. Hong, Y.-H. Kim and C. M. Koo, Large-area reduced graphene oxide thin film with excellent thermal conductivity and electromagnetic interference shielding effectiveness, *Carbon*, 2015, **94**, 494–500.
24 A. Moyseowicz, D. Minta and G. Gryglewicz, Conductive polymer/graphene-based composites for next generation energy storage and sensing applications, *ChemElectroChem*, 2023, **10**(9), e202201145.
25 S. Chhetri and T. Kuila, Polymer composites with 3D graphene architectures as high-performance EMI shielding materials: a review, *RSC Appl. Polym.*, 2024, **2**(4), 507–533.
26 N. Bellier, P. Baipaywad, N. Ryu, J. Y. Lee and H. Park, Recent biomedical advancements in graphene oxide-and reduced graphene oxide-based nanocomposite nanocarriers, *Biomater. Res.*, 2022, **26**(1), 65.
27 N. H. Othman, M. C. Ismail, M. Mustapha, N. Sallih, K. E. Kee and R. A. Jaal, Graphene-based polymer nanocomposites as barrier coatings for corrosion protection, *Prog. Org. Coat.*, 2019, **135**, 82–99.
28 G. Reina, N. D. Q. Chau, Y. Nishina and A. Bianco, Graphene oxide size and oxidation degree govern its supramolecular interactions with siRNA, *Nanoscale*, 2018, **10**(13), 5965–5974.
29 A. Arzac, G. P. Leal, J. C. de la Cal and R. Tomovska, Water-Borne Polymer/Graphene Nanocomposites, *Macromol. Mater. Eng.*, 2017, **302**(1), 1600315.
30 Y. Fadil, S. C. Thickett, V. Agarwal and P. B. Zetterlund, Synthesis of graphene-based polymeric nanocomposites using emulsion techniques, *Prog. Polym. Sci.*, 2022, **125**, 101476.
31 Y. Fadil, L. N. M. Dinh, M. O. Y. Yap, R. P. Kuchel, Y. Yao, T. Omura, U. A. Aregueta-Robles, N. Song, S. Huang, F. Jasinski, S. C. Thickett, H. Minami, V. Agarwal and P. B. Zetterlund, Ambient-Temperature Waterborne Polymer/rGO Nanocomposite Films: Effect of rGO Distribution on Electrical Conductivity, *ACS Appl. Mater. Interfaces*, 2019, **11**(51), 48450–48458.

32 V. Agarwal, Y. Fadil, A. Wan, N. Maslekar, B. N. Tran, R. A. Mat Noor, S. Bhattacharyya, J. Biazik, S. Lim and P. B. Zetterlund, Influence of Anionic Surfactants on the Fundamental Properties of Polymer/Reduced Graphene Oxide Nanocomposite Films, *ACS Appl. Mater. Interfaces*, 2021, **13**(15), 18338–18347.

33 N. Yousefi, M. M. Gudarzi, Q. Zheng, S. H. Aboutalebi, F. Sharif and J.-K. Kim, Self-alignment and high electrical conductivity of ultralarge graphene oxide–polyurethane nanocomposites, *J. Mater. Chem.*, 2012, **22**(25), 12709–12717.

34 S. H. Che Man, S. C. Thickett, M. R. Whittaker and P. B. Zetterlund, Synthesis of polystyrene nanoparticles "armoured" with nanodimensional graphene oxide sheets by miniemulsion polymerization, *J. Polym. Sci., Part A: Polym. Chem.*, 2013, **51**(1), 47–58.

35 S. H. Che Man, N. Y. Mohd Yusof, M. R. Whittaker, S. C. Thickett and P. B. Zetterlund, Influence of monomer type on miniemulsion polymerization systems stabilized by graphene oxide as sole surfactant, *J. Polym. Sci., Part A: Polym. Chem.*, 2013, **51**(23), 5153–5162.

36 Y. Fadil, F. Jasinski, T. Wing Guok, S. C. Thickett, H. Minami and P. B. Zetterlund, Pickering miniemulsion polymerization using graphene oxide: effect of addition of a conventional surfactant, *Polym. Chem.*, 2018, **9**(24), 3368–3378.

37 A. Domínguez, A. Fernández, N. González, E. Iglesias and L. Montenegro, Determination of critical micelle concentration of some surfactants by three techniques, *J. Chem. Educ.*, 1997, **74**(10), 1227.

38 Y. Fadil, S. H. C. Man, F. Jasinski, H. Minami, S. C. Thickett and P. B. Zetterlund, Formation of homogeneous nanocomposite films at ambient temperature via miniemulsion polymerization using graphene oxide as surfactant, *J. Polym. Sci., Part A: Polym. Chem.*, 2017, **55**(14), 2289–2297.

39 Y.-H. Yu, Y.-Y. Lin, C.-H. Lin, C.-C. Chan and Y.-C. Huang, High-performance polystyrene/graphene-based nanocomposites with excellent anti-corrosion properties, *Polym. Chem.*, 2014, **5**(2), 535–550.

40 C. Yu, C.-F. Wang and S. Chen, Facile access to graphene oxide from ferro-induced oxidation, *Sci. Rep.*, 2016, **6**(1), 17071.

41 R. Al-Gaashani, A. Najjar, Y. Zakaria, S. Mansour and M. Atieh, XPS and structural studies of high quality graphene oxide and reduced graphene oxide prepared by different chemical oxidation methods, *Ceram. Int.*, 2019, **45**(11), 14439–14448.

42 S. H. Che Man, D. Ly, M. R. Whittaker, S. C. Thickett and P. B. Zetterlund, Nano-sized graphene oxide as sole surfactant in miniemulsion polymerization for nanocomposite synthesis: Effect of pH and ionic strength, *Polymer*, 2014, **55**(16), 3490–3497.

43 Y. Fadil, V. Agarwal, F. Jasinski, S. C. Thickett, H. Minami and P. B. Zetterlund, Electrically conductive polymer/rGO nanocomposite films at ambient temperature via miniemulsion polymerization using GO as surfactant, *Nanoscale*, 2019, **11**(14), 6566–6570.

44 S. C. Thickett and R. G. Gilbert, Emulsion polymerization: State of the art in kinetics and mechanisms, *Polymer*, 2007, **48**(24), 6965–6991.

45 P. B. Zetterlund and D. R. D'hooge, The nanoreactor concept: kinetic features of compartmentalization in dispersed phase polymerization, *Macromolecules*, 2019, **52**(21), 7963–7976.

